Simultaneous detection of vertical and lateral forces by bimodal AFM utilizing quartz tuning fork sensor with a long tip

Yuya Yamada, Takashi Ichii*, Toru Utsunomiya and Hiroyuki Sugimura

Department of Materials Science and Engineering, Graduate School of Engineering, Kyoto University, Kyoto 606-8501, Japan

E-mail: ichii.takashi.2m@kyoto-u.ac.jp

Abstract

Simultaneous detection of vertical and lateral forces at nanoscale by atomic force microscopy (AFM) provides important knowledge in nanotribology. Although silicon (Si) cantilevers are capable of detecting both the forces, it has not been achieved by quartz tuning fork (QTF) sensors including qPlus sensors. In this study, we found that the tip apex of the qPlus sensor with a long tip oscillates vertically at the lowest resonance frequency (f_1) and laterally at the second lowest resonance frequency (f_2) by the finite element method (FEM) simulation. The lateral oscillation was experimentally confirmed by atomic resolution imaging, where the imaged atoms were apparently connected as increasing the oscillating amplitude at f_2. We also demonstrated the nanometer-scale friction force measurement by using the developed bimodal AFM. The obtained result was in good agreement with the contact-mode lateral force microscopy utilizing a Si cantilever.

Key words

multifrequency atomic force microscopy, qPlus sensor, atomic resolution, nanotribology

1. Introduction

Atomic force microscopy (AFM)[1] is a powerful tool for structural analysis of solid surfaces or solid/liquid interfaces. It enables nanoscale imaging using force acting between a tip and surface. The silicon (Si) cantilevers utilizing an optical beam deflection technique are most widely used as the force sensor, where both the vertical deflection and lateral torsion of the cantilever are detected by a four-segment photodiode.[2] The vertical force is usually used for topographic imaging. In contrast, the lateral force reflects a friction force acting between the tip and surface.[3] Nanoscale and atomic scale analysis of friction is of crucial importance for nanotribology.[4,5] Recently, S. Kawai and coworkers demonstrated vertical and lateral bimodal AFM, which uses lowest flexural and torsional resonance modes of a Si cantilever, in an ultrahigh vacuum (UHV) environment.[6–8] They achieved simultaneous detection of the vertical force and the atomically resolved lateral force.

In addition to Si cantilevers, quartz tuning fork (QTF) sensors, especially qPlus sensors,[9] are also widely used as the AFM force sensor. The qPlus sensor with a tip attached perpendicularly to the QTF beam has exhibited atomic resolution in various environments, such as UHV,[10] ambient air[11,12] and liquids.[13,14] The qPlus sensor can also detect the lateral force by attaching a tip parallel to the long axis of the QTF beam.[15–17] However, simultaneous detection of vertical and lateral forces by a qPlus sensor is difficult because torsional deformation of QTF is undetectable by its piezoelectric effect. Therefore, simultaneous excitation of flexural and torsional modes similar to Si cantilevers is useless for qPlus sensors. To the best of our knowledge, the only one report of atomic resolution bimodal AFM by a qPlus sensor has been published, where the tip apex oscillates in the vertical direction at both the two resonance frequencies.[18] A different design of a quartz sensor, that uses first two flexural modes of the quartz beam supported at both ends and a tip is attached at center of the beam, was proposed to detect vertical and lateral forces simultaneously.[19] However, no experiments has been demonstrated with this sensor. A short tip with a small mass is widely used for QTF sensors because a mass of the tip decreases the resonance frequency of the QTF, which generally suppresses the force sensitivity and complicates the motion of QTF.

In this report, the qPlus sensor with a long tip (> 1 mm) attached perpendicularly to the long axis of the QTF beam was adopted. It was found that the tip apex of the sensor oscillates vertically at the lowest resonance frequency, f_1, and laterally at the second lowest resonance frequency, f_2, by the finite element method (FEM) simulation. We demonstrated atomic resolution imaging of KBr(100) and nanometer-scale friction force measurements on

graphene oxide (GO) sheets spincoated on a highly oriented pyrolytic graphite (HOPG) substrate by the bimodal AFM using f_1 and f_2 of the qPlus sensor. In the atomic resolution images, the atoms of a KBr(100) surface were apparently connected when the oscillating amplitude at f_2 increased. This indicates that the tip apex oscillates laterally at f_2. In the bimodal AFM results of the GO-coated HOPG substrate, the GO-covered area showed larger energy dissipation compared to the bare HOPG surface at f_2, which is in good agreement with contact-mode lateral force microscopy (LFM) utilizing a Si cantilever. These simulation and experimental results revealed that the lateral friction force is simultaneously detectable with the vertical force by a qPlus sensor with a long tip.

2. Experimental methods

Figure 1 shows a photograph of a qPlus sensor used in this study. One prong of a commercial quartz tuning fork (QTF, STATEK Co., TFW 1165, spring constant 1884 N m^{-1}) was bound to a mount. A tungsten wire (The Nilaco Co., diameter 0.1 mm) was electrochemically etched in potassium hydroxide aqueous solution (1.2 mol L^{-1}) and glued to the other prong by EPO-TEK H70E (Epoxy Technology, Inc.). The length of the tungsten tip was 1.2-1.5 mm, which is relatively larger than the typical value used in qPlus sensors.

FEM simulation was carried out by FreeCAD 0.17,[20] an open source 3D parametric modeler with FEM solvers, in order to reveal the oscillation modes of the qPlus sensor numerically. Table I shows physical parameters of the QTF and the tungsten tip. It was approximated that the QTF and the tip were bonded by a plane and the QTF except for the prong with the tip was fixed. Creation of a mesh and solution of resonance modes were conducted by Gmsh and Calculix on FreeCAD.

The experiment was performed by a system based on a commercial AFM (JEOL, JSPM-5200) of which original AFM head was replaced by a home-built AFM head made for a qPlus sensor. Figure 2 shows a block diagram of the bimodal AFM setup. The sensor was mechanically oscillated by lead zirconate titanate (PZT) piezoelectric plate driven at two different resonance frequencies simultaneously. The deflection signal of the sensor was amplified by a differential current amplifier[21] embedded in the AFM head. Frequency shift of the lowest resonance frequency (Δf_1) was detected by a commercial FM demodulator (Kyoto Instruments, KI-2001) with some modifications, and amplitude and phase shift at the second lowest resonance frequency (A_2, φ_2) were detected by lock-in amplifier (NF Electronic Instruments, LI 5640). Topographic images were obtained as two-dimensional maps of the tip trajectory where Δf_1 was kept constant, which is so-called frequency

modulation (FM) mode.

A KBr(100) substrate was used as a standard sample for atomic resolution imaging. 1-Butyl-3-methylimidazolium hexafluorophosphate (BMIM-PF_6, > 98 %) was purchased from Tokyo Chemical Industry Co., Ltd. and used without further purification. The saturated KBr solution of BMIM-PF_6 was prepared by adding 1 wt% of KBr powder (Nacalai Tesque Inc., > 99 %) and agitating on a tube rotator for 1 day. After that, (100) oriented KBr single crystal (Furuuchi Chemical Co.) was cleaved by using sharp knife and immediately supernatant of the solution (0.5 μL) was dropped on the cleaved KBr(100) surface. This sample was left in the dry chamber (dew point < -50 °C) for 1 day, and then it was investigated by the bimodal AFM with the long tip qPlus sensor.

GO and graphite were used as a test sample for friction force measurements in ionic liquid. GO sheets were prepared through a modified Hummers' method.[22] A highly oriented pyrolytic graphite (HOPG, SPI supplies, SPI-2 grade, 10 x 10 x 2 mm) was cleaved by using scotch tape, and then the GO 1-propanol dispersion was spincoated onto the cleaved HOPG surface. 1-Ethyl-3-methylimidazolium bis(trifluoromethylsulfonyl)imide (EMIM-Tf_2N, purchased from Kanto Chemical Co., Inc.) 0.5 μL was dropped on the substrate, and then the sample was investigated by the bimodal AFM using another qPlus sensor.

3 Results and discussion

Figure 3 shows thermal Brownian spectra of the qPlus sensor obtained in ambient air. The frequencies of the first two resonance modes were f_1 = 13.509 kHz and f_2 = 160.760 kHz. The quality factors (Q factors) of f_1 and f_2 were 2439 and 423 respectively. These two resonance modes were adopted to this bimodal AFM experiment. The 2nd resonance frequency, f_2, was 11.9 times higher than f_1. It is quite different from theoretical values of cantilever's 2nd and 3rd resonance frequencies (6.27 times and 17.6 times of f_1), because higher resonance modes of qPlus sensors are drastically affected by mass and rotation inertia of the long tip.[23] Considering that, resonance frequencies and modes were calculated by the method in Ref. 23. In this method only in-plane oscillations (vertical oscillations) of the QTF were considered. The tip was approximated as a rigid circular column length of 1.17 mm in order to equalize its mass to the actual amount. The solutions of first three resonance frequencies were 13.8 kHz, 64.2 kHz and 240 kHz, and the oscillation modes of them are shown in Fig. 4. That is in good agreement with the experimental values of f_1 but not f_2, which suggests the possibility that the tip doesn't behave as a rigid body at f_2. In fact, the spring constant of the tip is 2730 N m^{-1} (calculated by approximating the tip as a circular

column), which is the same in the order of magnitude as that of the QTF beam in the in-plane direction, 1884 N m^{-1}. Furthermore, the spring constants of higher resonance modes are generally much higher than that of the fundamental mode. Therefore, the rigid-tip approximation was not suitable in this case. The results also suggested the presence of out-of-plane or torsional oscillation modes. These modes, however, are considered less likely to be detected by piezoelectric effect of QTFs because they are manufactured for sensing in-plane oscillation.

The calculated frequencies at higher resonance modes under the rigid-tip approximation are obviously different from the experimental values. In order to investigate resonance modes of the qPlus sensor more exactly, FEM simulation was carried out by FreeCAD. The tip attached to the qPlus sensor had tilted 8° from the perpendicular direction of the QTF beam (Fig. 5 (a)), which was reflected in the simulation model (Fig. 5 (b)). The simulation results of first six resonance frequencies were obtained at 7.94 kHz, 13.4 kHz, 32.6 kHz, 43.5 kHz, 94.0 kHz and 162 kHz, and the oscillation modes of them are shown in Fig. 5 (c)-(h). The frequencies of the oscillation modes shown in Fig. 5 (d) and (h) agrees well to the experimental values of f_1 and f_2 respectively, and the QTF vertically oscillates at both f_1 and f_2. Although the simulation suggests that the QTF oscillates in the in-plane direction at 43.5 kHz (Fig. 5 (f)), the deflection signal of this mode was not detected by its piezoelectric effect. This is ascribed that this mode mostly consists of the tip oscillation and the QTF oscillation is negligibly small. The others consist of out-of-plane or torsional oscillation, which were not detectable by the piezoelectric effect. Figure 5 (i) and (j) are side views of resonance modes at f_1 and f_2 (Fig. 5 (d) and (h)), respectively. According to them, the tip also bends at f_2 and the tip apex oscillates in a direction orthogonal to that of f_1. The deflection of the QTF end at f_2 was relatively small, and the tip bended to +x (-x) direction when middle part of the QTF deflected to +z (-z) direction. Figure 5 (k) is the image of the tip apex displacement at f_2 viewed from a side. The misalignment from the lateral direction was 7°, which indicates that the crosstalk of vertical force was suppressed to ~12 % and the lateral force was dominantly detected. Note that, we also found that the misalignment can be decreased to 1° by elongating the tip length to 2 mm, where the crosstalk is suppressed less than 2 %. Figure 5 (l) is the image of the 2nd resonance mode at f_2 viewed from the bottom. It was found that the angle formed by the direction of the tip apex oscillation and the long axis of the QTF is about 30°. This is probably because the tip was attached on the side of the QTF and that made some torque around the long axis of the QTF. Additionally, we have also confirmed that the effect of the adhesive on the oscillation modes was

negligibly small. At this stage, it is considered that the tip apex oscillates in the lateral direction at f_2, while it is difficult to interpret the deflection signal of f_2 to its actual amplitude because of the complex coupled motion of the QTF and the tip.

In the FEM simulation, the tip apex of qPlus sensor with a long tip oscillates vertically at f_1 and laterally at f_2. In order to experimentally confirm this simulation result, atomic resolution imaging was conducted by the bimodal AFM with the qPlus sensor. Figure 6 (a)-(d) are atomically resolved KBr(100) surface images and their Fast Fourier Transform (FFT) patterns obtained with the same fast scan direction in the saturated KBr solution of BMIM-PF_6. KBr has a rock-salt structure with a lattice constant a = 660 pm (Fig. 6 (e)). Figure 6 (a) was obtained by operating only 1st mode with the amplitude A_1=180 pm. The square-lattice bright spots with the lattice spacing of 475 pm were clearly imaged, which are in good agreement with the spacing between equally charged ions, $\frac{a}{\sqrt{2}}$. Thus, the bright spots represent the periodic sites of only one atomic species as described at previous reports.[11,18,24] Figure 6 (b), (c) and (d) were obtained by bimodal AFM operating with constant A_1 (180 pm) and various A_2 (28.3 mV, 56.5 mV and 113 mV). The lateral amplitude A_2 are described by the detected signal voltage because interpretation from the voltage to the actual lateral amplitude has not been achieved. Although the separated bright spots forming a square-lattice structure were imaged in Fig. 6 (a) and (b), the image changed to stripe-like patterns as A_2 was increased, which can be also confirmed in the FFT patterns. That is, the imaged atoms were apparently connected to each other. These results are quite different from the previous report in which a short tip was used.[18] In atomic resolution images obtained by dynamic LFM (DLFM)[25] and scanning tunneling microscopy (STM) combined with DLFM[16,26,27] in which the tip apex oscillates laterally, neighboring atoms in the direction of the tip dithering were apparently connected. It should be noted that the AFM images obtained in this experiment are flipped upside down because of our instrumental setting. In order that, the direction of the observed stripes corresponds well to the direction of the tip apex oscillation in the FEM simulation (Fig. 5 (l)). Therefore, these experimental results revealed that the tip apex oscillates laterally at f_2. In addition, considering the fact that atoms were separately imaged in Fig.6 (b) with A_2 = 28.3 mV and were apparently connected in (c) with A_2 = 56.5 mV, the actual lateral amplitude of the tip apex at f_2 can be roughly estimated to be the same order as the lattice spacing.

It was confirmed by the atomic resolution imaging of KBr(100) that the tip apex of a qPlus sensor with a long tip oscillates laterally at f_2. The next step is the simultaneous detection of vertical and lateral forces by the bimodal AFM. Figure 7 (a)-(c) show bimodal AFM results

of the GO-coated HOPG substrate obtained in EMIM-Tf_2N with another qPlus sensor (tip length 1.68 mm, f_1 = 11.222 kHz, f_2 = 133.46 kHz). We found that many protrusions were distributed only in the upper area of the topographic image (Fig. 7 (a)). These are typical structures of GO sheets, which are originated from the oxygen functional groups and the defects.[28] Thus we can conclude that the upper area and the lower area correspond to the GO-covered area and the bare HOPG surface, respectively. The GO-covered area exhibits larger amplitude attenuation and phase shift of the 2nd mode compared to the HOPG area as shown in Fig. 7 (b) and (c). We also found that the height variation in the bare HOPG did not affect the amplitude and the phase of the 2nd mode, which indicated that the surface properties are detected by the 2nd mode without topographic effects. In dynamic-mode AFM, the energy dissipated by the tip-sample interaction (E_{dis}) is given by[29]

$$E_{\mathrm{dis}} = \frac{\pi k A^2 f}{Q}\left(\frac{Q A_{\mathrm{d}}}{A}\sin(-\varphi) - \frac{f}{f_0}\right),$$

where k, Q, A_{d} and f_0 are spring constant, quality factor, driving amplitude and natural frequency of the sensor, respectively. Then, A, φ and f represent amplitude, phase shift and frequency when the tip approaches the surface. Since $f \simeq f_0$ and QA_{d} is equal to free amplitude at resonance frequency (A_0), E_{dis} can be approximated as

$$E_{\mathrm{dis}} = \frac{\pi k A^2 f_0}{Q}\left(\frac{A_0}{A}\sin(-\varphi) - 1\right).$$

Although the absolute value of the energy dissipation cannot be determined because the actual lateral amplitude is unknown, the ratio of the energy dissipation on GO and HOPG can be derived by using the above equation. According to the histograms (Fig. 7 (d), (e)), the averaged amplitude and the averaged phase shift of the 2nd mode on the GO-covered area were 11.43 mV and -89.27°, and those on the bare HOPG area were 11.68 mV and -89.88°. Substituting them into the above equation, we got $E_{\mathrm{dis\,GO}} = 2.1\,E_{\mathrm{dis\,HOPG}}$. The energy dissipation in the lateral oscillation can be originated from the friction force acting between the tip and the surface by considering the motion equation. Therefore, we concluded that larger friction force was detected on GO sheets than on HOPG by the bimodal AFM. The result was in qualitative agreement with that of a previous report by contact-mode LFM utilizing diamond-like carbon (DLC)-coated Si cantilever, where GO showed larger friction force than HOPG.[30] Thus, it is considered that vertical and lateral forces are simultaneously detectable by the bimodal AFM using the qPlus sensor with a long tip.

4. Conclusion

We demonstrated simultaneous detection of vertical and lateral forces by the bimodal AFM utilizing a qPlus sensor with a long tip. It was found that the tip apex of the qPlus sensor oscillates laterally at f_2 by FEM simulation, and it was confirmed by atomic resolution imaging of KBr(100) surface. Friction force on the GO-coated HOPG substrate in EMIM-Tf_2N was detected by the bimodal AFM, and the results agreed well to the contact-mode LFM study. It is remarkable that vertical and lateral forces are detectable by the qPlus sensor without special modifications.

This method would be quite useful for nanoscale analysis of lubrication. Structural analysis of lubricant-solid interface has been performed by FM-AFM, and the lubrication layer was visualized.[31,32)] As a further study, the direct detection of the lateral force at the interface will be achieved by this bimodal AFM. The quantitative detection of lateral force is necessary for these applications. Further research is required for calibration of the actual lateral amplitude, decrease of the misalignment from the lateral direction and quantification of the detected lateral force.

Acknowledgement

This work was supported by a Grant-in-Aid for Scientific Research B (No. 17H02787) from Japan Society for Promotion of Science (JSPS).

References

1) G. Binnig, C.F. Quate, and C. Gerber, Phys. Rev. Lett. **56**, (1986)

2) G. Meyer and N.M. Amer, Appl. Phys. Lett. **57**, 2089 (1990)

3) C.M. Mate, G.M. McClelland, R. Erlandsson, and S. Chiang, Phys. Rev. Lett. **59**, 1942 (1987)

4) B. Bhushan, J.N. Israelachvili, and U. Landman, Nature **374**, 607 (1995)

5) G.V. Dedkov, Uspekhi Fiz. Nauk **170**, 585 (2000)

6) S. Kawai, F.F. Canova, T. Glatzel, T. Hynninen, E. Meyer, and A.S. Foster, Phys. Rev. Lett. **109**, 146101 (2012)

7) S. Kawai, T. Glatzel, S. Koch, B. Such, A. Baratoff, and E. Meyer, Phys. Rev. B **81**, 085420 (2010)

8) F. Federici Canova, S. Kawai, C. de Capitani, K. Kan'no, T. Glatzel, B. Such, A.S. Foster, and E. Meyer, Phys. Rev. Lett. **110**, 203203 (2013)

9) F.J. Giessibl, Appl. Phys. Lett. **73**, 3956 (1998)

10) F.J. Giessibl, Appl. Phys. Lett. **76**, 1470 (2000)

11) D.S. Wastl, A.J. Weymouth, and F.J. Giessibl, Phys. Rev. B **87**, 245415 (2013)

12) D.S. Wastl, A.J. Weymouth, and F.J. Giessibl, ACS Nano **8**, 5233 (2014)

13) T. Ichii, M. Fujimura, M. Negami, K. Murase, and H. Sugimura, Jpn. J. Appl. Phys. **51**, 08KB08 (2012)

14) T. Ichii, M. Negami, and H. Sugimura, J. Phys. Chem. C **118**, 26803 (2014)

15) F.J. Giessibl, M. Herz, and J. Mannhart, Proc. Natl. Acad. Sci. **99**, 12006 (2002)

16) A.J. Weymouth, D. Meuer, P. Mutombo, T. Wutscher, M. Ondracek, P. Jelinek, and F.J. Giessibl, Phys. Rev. Lett. **111**, 126103 (2013)

17) A.J. Weymouth, E. Riegel, S. Matencio, and F.J. Giessibl, Appl. Phys. Lett. **112**, 181601 (2018)

18) H. Ooe, D. Kirpal, D.S. Wastl, A.J. Weymouth, T. Arai, and F.J. Giessibl, Appl. Phys. Lett. **109**, 141603 (2016)

19) J. Stirling, Beilstein J. Nanotechnol. **4**, 370 (2013)

20)"FreeCAD", https://www.freecad.io

21) F. Huber and F.J. Giessibl, Rev. Sci. Instrum. **88**, 073702 (2017)

22) M. Hirata, T. Gotou, S. Horiuchi, M. Fujiwara, and M. Ohba, Carbon N. Y. **42**, 2929 (2004)

23) R.C. Tung, T. Wutscher, D. Martinez-Martin, R.G. Reifenberger, F. Giessibl, and A. Raman, J. Appl. Phys. **107**, 104508 (2010)

24) S. Kawai, T. Glatzel, S. Koch, B. Such, A. Baratoff, and E. Meyer, Phys. Rev. Lett. **103**, 220801 (2009)
25) S. Kawai, S. Kitamura, D. Kobayashi, and H. Kawakatsu, Appl. Phys. Lett. **87**, 173105 (2005)
26) S. Kawai, N. Sasaki, and H. Kawakatsu, Phys. Rev. B **79**, 195412 (2009)
27) N. Sasaki, S. Kawai, and H. Kawakatsu, Phys. Rev. B **80**, 193402 (2009)
28) S. Katano, T. Wei, T. Sasajima, R. Kasama, and Y. Uehara, Phys. Chem. Chem. Phys. **20**, 17977 (2018)
29) J.P. Cleveland, B. Anczykowski, A.E. Schmid, and V.B. Elings, Appl. Phys. Lett. **72**, 2613 (1998)
30) D. Berman, A. Erdemir, A. V. Zinovev, and A. V. Sumant, Diam. Relat. Mater. **54**, 91 (2015)
31) T. Hirayama, R. Kawamura, K. Fujino, T. Matsuoka, H. Komiya, and H. Onishi, Langmuir **33**, 10492 (2017)
32) H. Okubo and S. Sasaki, Tribol. Lett. **67**, 3 (2019)

Figure captions

Fig. 1. A photograph of a qPlus sensor

Fig. 2. A schematic diagram of the bimodal AFM setup in this work. Frequency shift of 1st mode (Δf_1) was detected by the frequency detector, and topographic images were obtained as two-dimensional tip trajectories, where Δf_1 was kept constant. Amplitude and phase shift of 2nd mode (A_2, φ_2) were observed by a lock-in amplifier.

Fig. 3. Thermal noise spectra of the qPlus sensor obtained in ambient air (a) around 1st resonance frequency (f_1 = 13.509 kHz, Q_1 = 2439) (b) around 2nd resonance frequency (f_2 = 160.760 kHz, Q_2 = 423)

Fig.4. Calculation results of resonance modes obtained by the method in Ref. 23 approximating the tip as a rigid circular column. The solutions of first three resonance frequencies were 13.8 kHz (red solid line), 64.2 kHz (blue broken line) and 240 kHz (green dashed dotted line).

Fig. 5. (a) A optical microscope image of the tip attached to the qPlus sensor used in this experiment. The tip was tilted 8° from the long axis of the QTF. (b) A 3D parametric model of the qPlus sensor. Red bodies indicated fixed boundary condition. (c)-(h) FEM simulation results of resonance modes. First six resonance frequencies were 7.94 kHz (c, out-of-plane), 13.4 kHz (d, in-plane), 32.6 kHz (e, torsion), 43.5 kHz (f, in-plane and tip-bending), 94.0 kHz (g, out-of-plane and tip-bending) and 162 kHz (h, in-plane and tip-bending). (i) The side view of (d). (j) The side view of (h). (k) The tip apex of (h) viewed from a side. The misalignment from lateral direction is 7°. (l) The tip apex of (h) viewed from bottom. The dithering direction of the tip apex tilted 30° from the long axis of the quartz beam.

Fig. 6. (a)-(d) Topographic images and its FFT patterns of KBr(100) obtained in KBr-saturated BMIM-PF_6 by the bimodal AFM with constant A_1 (180 pm) and different A_2.

Δf_1 was kept constant during each imaging. (a) A_2 = 0 mV, Δf_1 = +250 Hz (b) A_2 = 28.3 mV, Δf_1 = +280 Hz (c) A_2 = 56.5 mV, Δf_1 = +290 Hz (d) A_2 = 113 mV, Δf_1 = +260 Hz (e) A schematic illustration of KBr(100) surface and the tip dithering direction at f_2

Fig. 7. The friction measurement result of the GO-coated HOPG substrate obtained in EMIM-Tf_2N. (a) Topography, (b) 2nd mode amplitude, (c) 2nd mode phase, They were obtained with A_1 = 190 pm, A_2 = 11.9 mV and Δf_1 = +82 Hz. (d) Histogram of (b), (e) Histogram of (c), The red and blue curves are results of fitting with Gaussian functions.

Table

Table I. The physical properties of the QTF and the tungsten tip used for the calculation and the FEM simulation.

quartz tuning fork		tungsten tip	
Young's modulus	80 GPa	Young's modulus	345 GPa
Poisson's ratio	0.17	Poisson's ratio	0.284
density	2.65 g/cm^3	density	19.25 g/cm^3
beam width	0.213 mm	length	1.33 mm
beam length	2.357 mm	diameter	0.1 mm
beam thickness	0.127 mm		

Figures

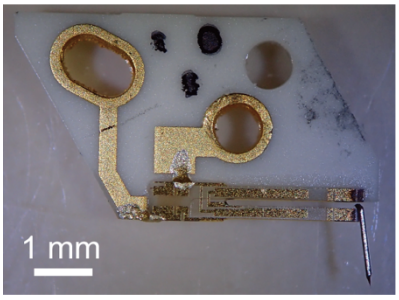

Fig. 1

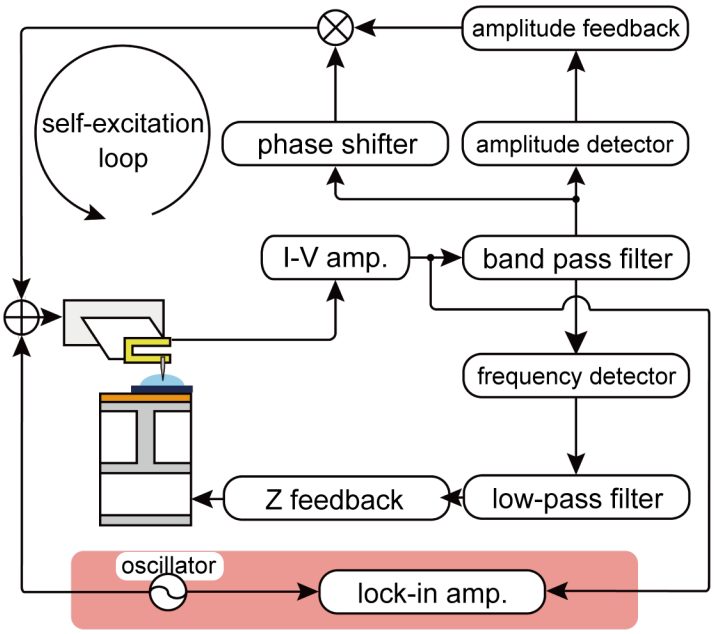

Fig. 2

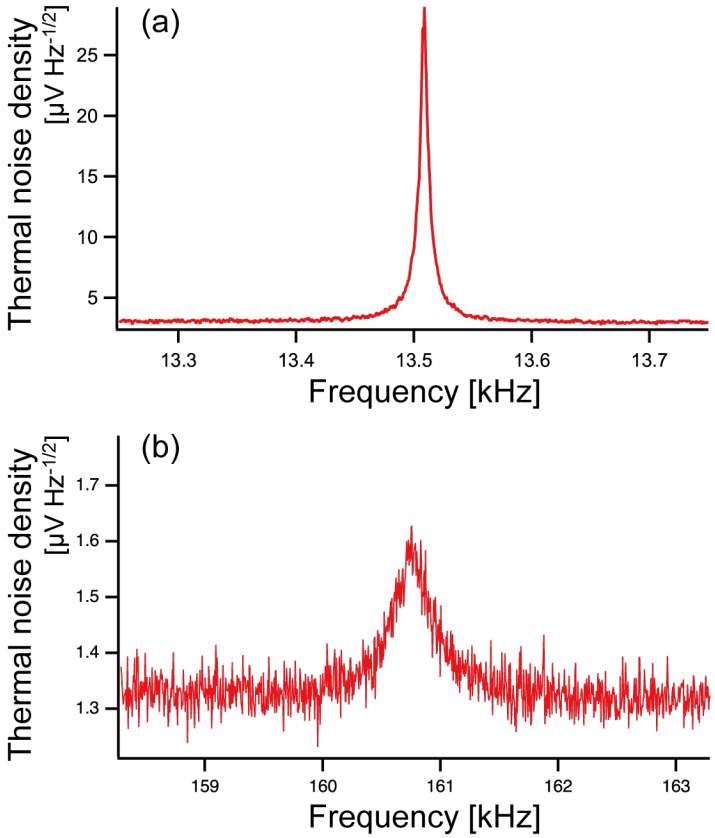
(a)
Thermal noise density
[μV Hz-1/2]
25
20
15
10
5
13.3
13.4
13.5
13.6
13.7
Frequency [kHz]
(b)
Thermal noise density
[μV Hz-1/2]
1.7
1.6
1.5
1.4
1.3
159
160
161
162
163
Frequency [kHz]

Fig. 3

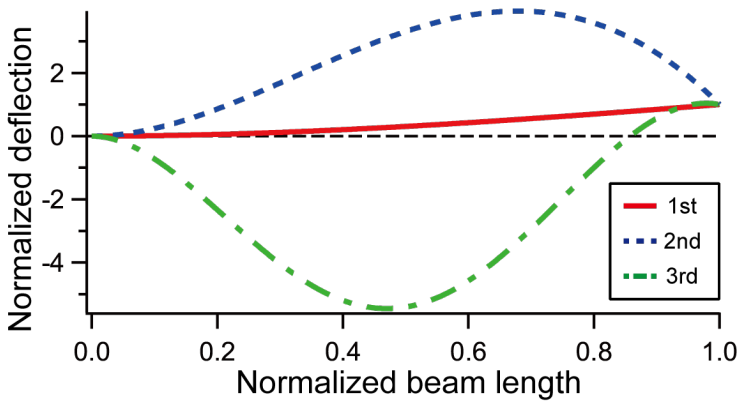
Normalized deflection
2
0
-2
-4
0.0
0.2
0.4
0.6
0.8
1.0
Normalized beam length
1st
2nd
3rd

Fig.4

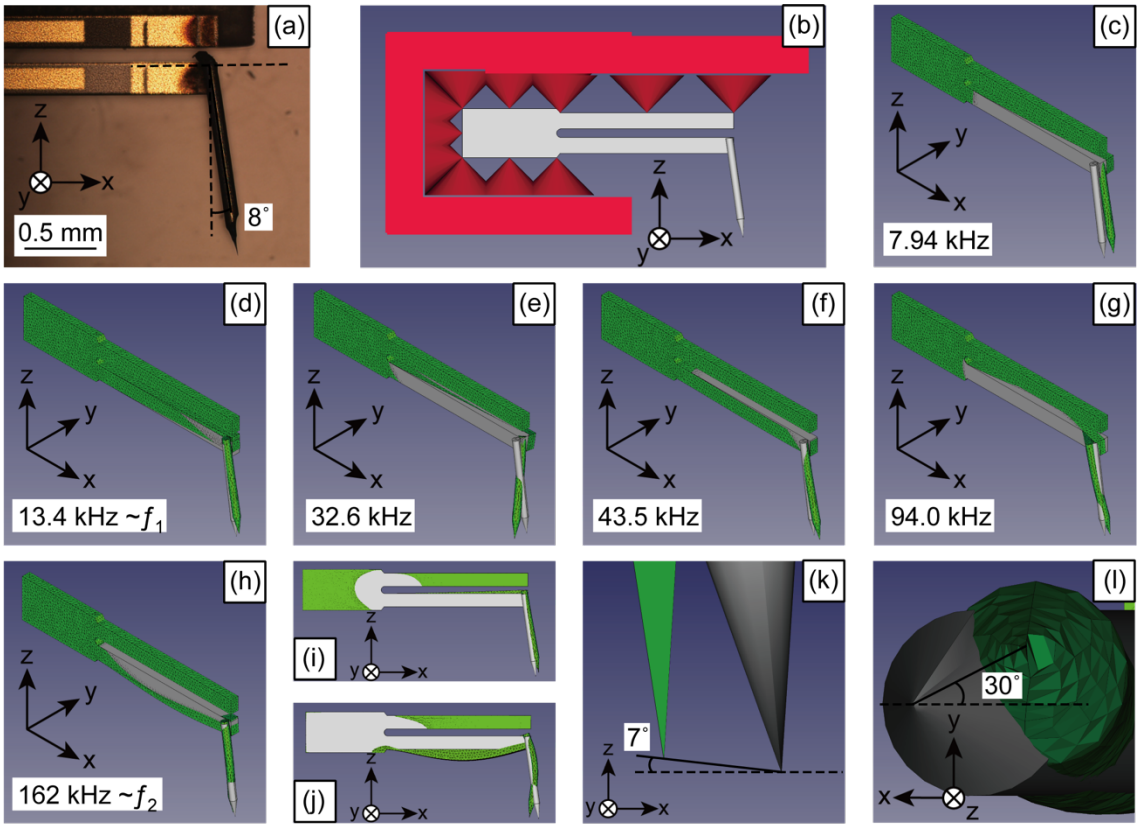
(a)
0.5 mm
8°
(b)
(c)
7.94 kHz
(d)
13.4 kHz ~f_1
(e)
32.6 kHz
(f)
43.5 kHz
(g)
94.0 kHz
(h)
162 kHz ~f_2
(i)
(j)
(k)
7°
(l)
30°

Fig. 5

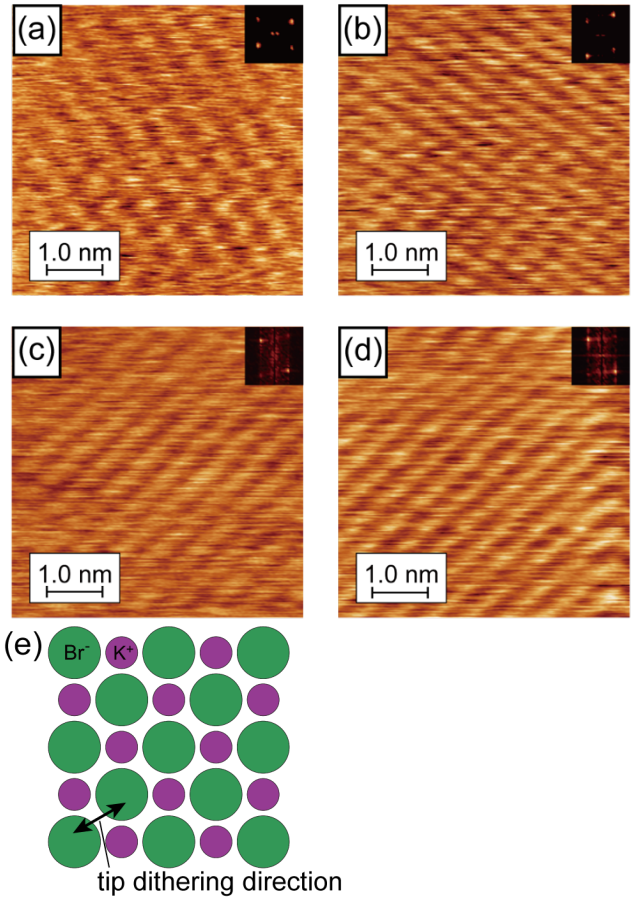
(a)
1.0 nm
(b)
1.0 nm
(c)
1.0 nm
(d)
1.0 nm
(e)
Br⁻
K⁺
tip dithering direction

Fig. 6

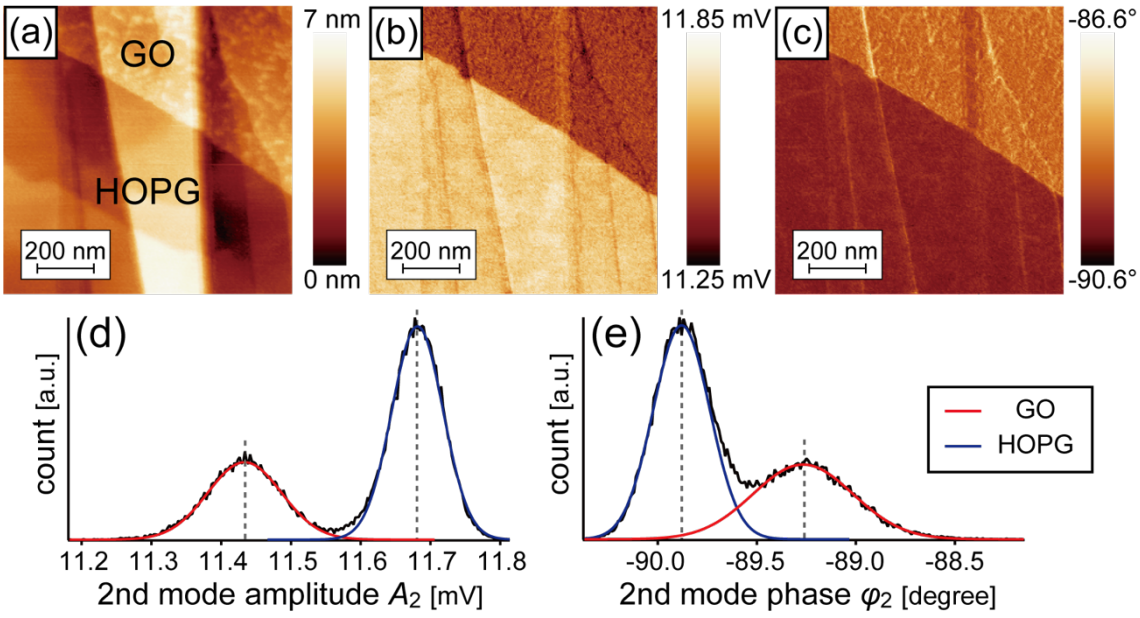
(a)
GO
HOPG
200 nm
7 nm
0 nm
(b)
200 nm
11.85 mV
11.25 mV
(c)
200 nm
-86.6°
-90.6°
(d)
count [a.u.]
11.2 11.3 11.4 11.5 11.6 11.7 11.8
2nd mode amplitude A_2 [mV]
(e)
count [a.u.]
-90.0 -89.5 -89.0 -88.5
2nd mode phase φ_2 [degree]
GO
HOPG

Fig. 7